ELSEVIER

Earth and Planetary Science Letters 121 (1994) 81–98

EPSL

Magnetostratigraphic, lithostratigraphic and tephrostratigraphic constraints on Lower and Middle Pleistocene sea-level changes, Wanganui Basin, New Zealand

Brad J. Pillans [a], Andrew P. Roberts [b], Gary S. Wilson [a], Stephen T. Abbott [c], Brent V. Alloway [d]

[a] *Research School of Earth Sciences, Victoria University of Wellington, P.O. Box 600, Wellington, New Zealand*
[b] *Department of Geology, University of California, Davis, CA 95616, USA*
[c] *Department of Geology, University of Tasmania, P.O. Box 252C, Hobart 7001, Tasmania, Australia*
[d] *Department of Geology, University of Auckland, Private Bag 92019, Auckland, New Zealand*

(Received December 11, 1992; revision accepted October 10, 1993)

Abstract

Wanganui Basin, North Island, New Zealand, contains a complex sedimentary record of Lower and Middle Pleistocene sea-level changes. Palaeomagnetic results allow identification of the Matuyama/Brunhes transition, the Jaramillo Subchron and the Cobb Mountain Subchron. Correlations of rhyolitic tuff horizons across the basin are consistent with magnetostratigraphic correlations between sections. Isothermal plateau fission-track (ITPFT) ages of 1.05 ± 0.05 Ma and 1.63 ± 0.15 Ma on two tuffs (Potaka Pumice and Pakihikura Pumice, respectively) are consistent with the interpreted magnetostratigraphy and also with the astronomically tuned timescale of ODP Site 677. Magnetostratigraphy and ITPFT ages allow correlation of sedimentary cycles at Wanganui with odd-numbered oxygen isotope stages 17–31 in deep-sea cores. The stratotype section for the New Zealand Castlecliffian Stage is shown to be incomplete relative to other studied sections in the basin. Below stage 31, the character of the cyclothems changes at Wanganui, from marine dominated, to a greater representation of non-marine and estuarine strata. This change may be partly related to a change in amplitude and frequency of climatic cycles identified in oxygen isotope records, but the primary cause is likely to be increased basinal uplift.

1. Introduction

Thick successions of cyclic Pleistocene marine sediment are well exposed onshore in the Wanganui Basin, southwestern North Island, New Zealand. These sediments provide an excellent opportunity to study geological records of sea-level change because coastal cliffs and stream sections provide extensive exposure across the basin. The sediments are richly fossiliferous and contain molluscan faunas that facilitate accurate analysis of sedimentary environments. A set of unconformity bound sequences [1], clearly displaying sedimentary facies characteristic of transgressive, maximum flooding and high-stand phases of sea level [2], can be traced more than 50 km across the basin. These strata are locally impor-

[MK]

SSDI 0012-821X(93)E0220-E

tant because the Wanganui Basin contains the stratotype localities for the Pliocene and Pleistocene stages and substages of New Zealand [1,3]. One of the coastal sections was recently proposed as a possible international Lower/Middle Pleistocene boundary stratotype [4].

Several methods have been used to date the Wanganui sediments, including biostratigraphy [3], tephrostratigraphy, fission-track dating [5–7], oxygen isotopes [8] and magnetostratigraphy [9]. However, basinwide differences in thickness and texture of correlative units and the presence of numerous sequence bounding unconformities make lithostratigraphic correlation between sections difficult. Although a recent study of the Middle Pleistocene Castlecliffian Stage stratotype locality by Turner and Kamp [9] demonstrates that magnetostratigraphy provides important chronological and stratigraphic controls, their results also identified a number of significant problems. Principal among these was the apparent inconsistency between palaeomagnetic and previous lithological correlations within the basin. Here we extend their work, and present magnetostratigraphic, lithostratigraphic and tephrostratigraphic results from four successions of Early to Middle Pleistocene age. These results enable a definitive correlation to be made across the Wanganui Basin, and facilitate a detailed comparison with oxygen isotope records, and the tuned orbital chronology of deep-sea cores [10].

2. Geological setting

The Wanganui Basin contains up to 4 km of Plio/Pleistocene sediment, and is situated in a back-arc position with respect to the Australia–Pacific plate boundary in North Island, New Zealand (Fig. 1). Stern and Davey [11] attribute Plio-Pleistocene subsidence and sedimentation to locking of the underlying subducted Pacific Plate.

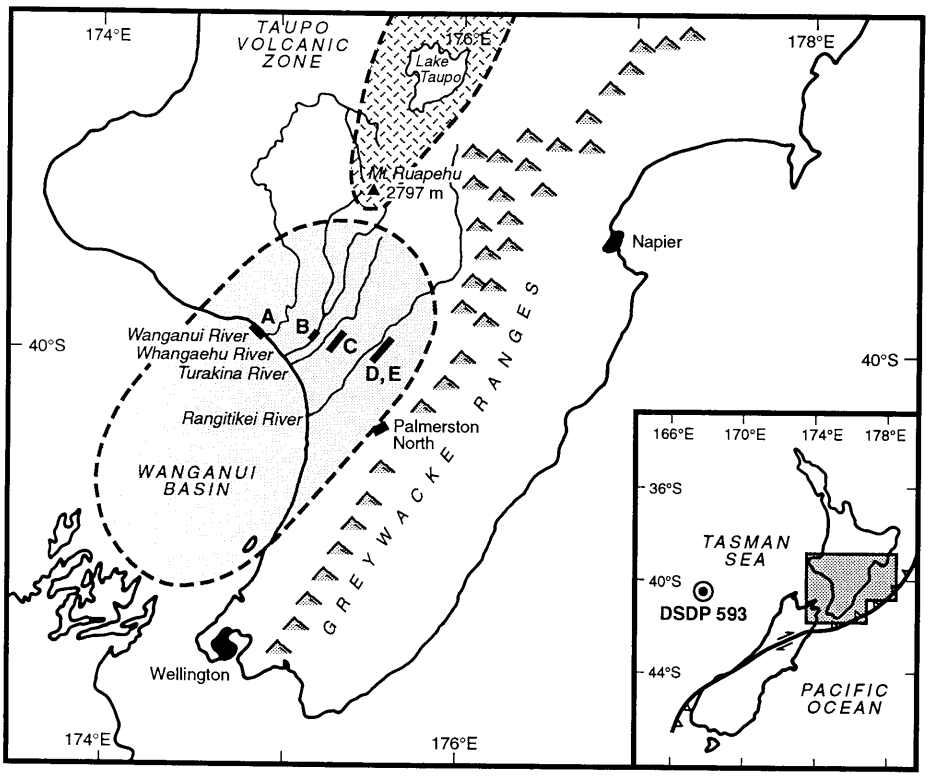

Fig. 1. Map of central New Zealand showing the Wanganui Basin and location of sections studied.

Back-arc volcanism in the Taupo Volcanic Zone (Fig. 1) has contributed substantial amounts of volcanigenic material to the basin, resulting in the deposition of numerous tephra horizons that can be dated and correlated. Uplift of the axial greywacke ranges of North Island has resulted in uplift of the eastern half of the Wanganui Basin above sea level (Fig. 1). Several major rivers drain the southern end of the volcanic plateau in central North Island, including the Wanganui, Whangaehu, Turakina and Rangitikei rivers. These rivers provide excellent exposure of Plio-Pleistocene strata in the basin. Exposed strata dip regionally south at 2–4°.

Pleistocene sedimentation in the Wanganui Basin occurred at a time of known large-amplitude glacioeustatic fluctuations in sea level [e.g., 12], and wave-cut marine terraces formed by transgressing seas during interglacial times are preserved around the basin margin [13]. Cyclical packages of unconformity-bound sequences of sediment in the Wanganui Basin [1] are interpreted to represent successive sea-level cycles [3,14]. Typically, these sequences consist of a basal erosional unconformity, succeeded by an open shoreface or tide-dominated sequence which often includes a cross-bedded shell conglomerate (Fig. 2). These sediments are interpreted to represent the transgressive part of the sequence. The overlying succession consists of a mid-cycle condensed shellbed, rich in offshore molluscan fossils, that is succeeded by a sparsely fossiliferous shelf siltstone which is usually truncated by the basal unconformity of the overlying sequence. The mid-cycle shellbeds are interpreted to have accumulated in an offshore, low-energy environment where a low input of terrigenous sediment allowed the growth, concentration and preservation of a relatively condensed shellbed [14]. The mid-cycle shellbed is therefore interpreted to be broadly equivalent to the maximum flooding surface of a sea-level cycle. Massive siltstones at the tops of cycles are interpreted as having been deposited during the sea-level high stand and, in some cases, part of the shoaling upwards cycle is preserved [14]. The sequence-bounding unconformities represent surfaces of marine planation cut by the landward passage of the shoreface of the transgressing sea. Typically, the thin package of sediment deposited during the sea-level low stand, and an unknown amount of the high-stand sediment of the underlying cycle, have been removed by erosion at the sequence bounding unconformities.

3. Tephrostratigraphy and tephrochronology

Volcaniclastic sediment occurs sporadically throughout the Wanganui Basin, much of which consists of virtually pure volcanic detritus [6]. These volcaniclastic sediments contain rhyolitic pumice, gravel and sand, derived by fluvial transport from large eruptions in the Taupo Volcanic Zone to the north (Fig. 1). Many of the volcaniclastic horizons (tuffs) are similar in field appear-

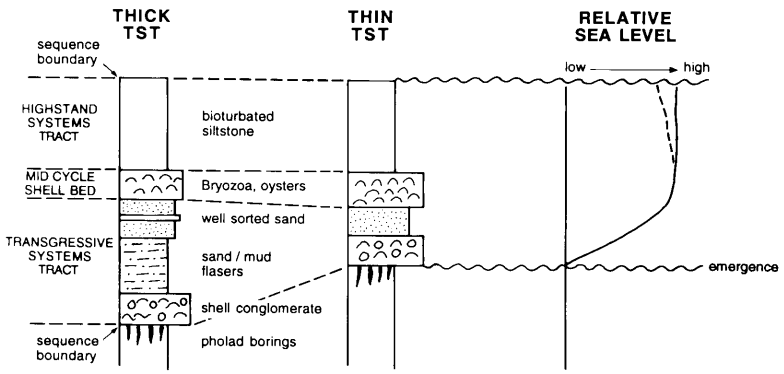

Fig. 2. Idealized cyclothems from Castlecliff section, Wanganui [after 14], and interpretation of relative sea-level changes. *TST* = transgressive systems tract.

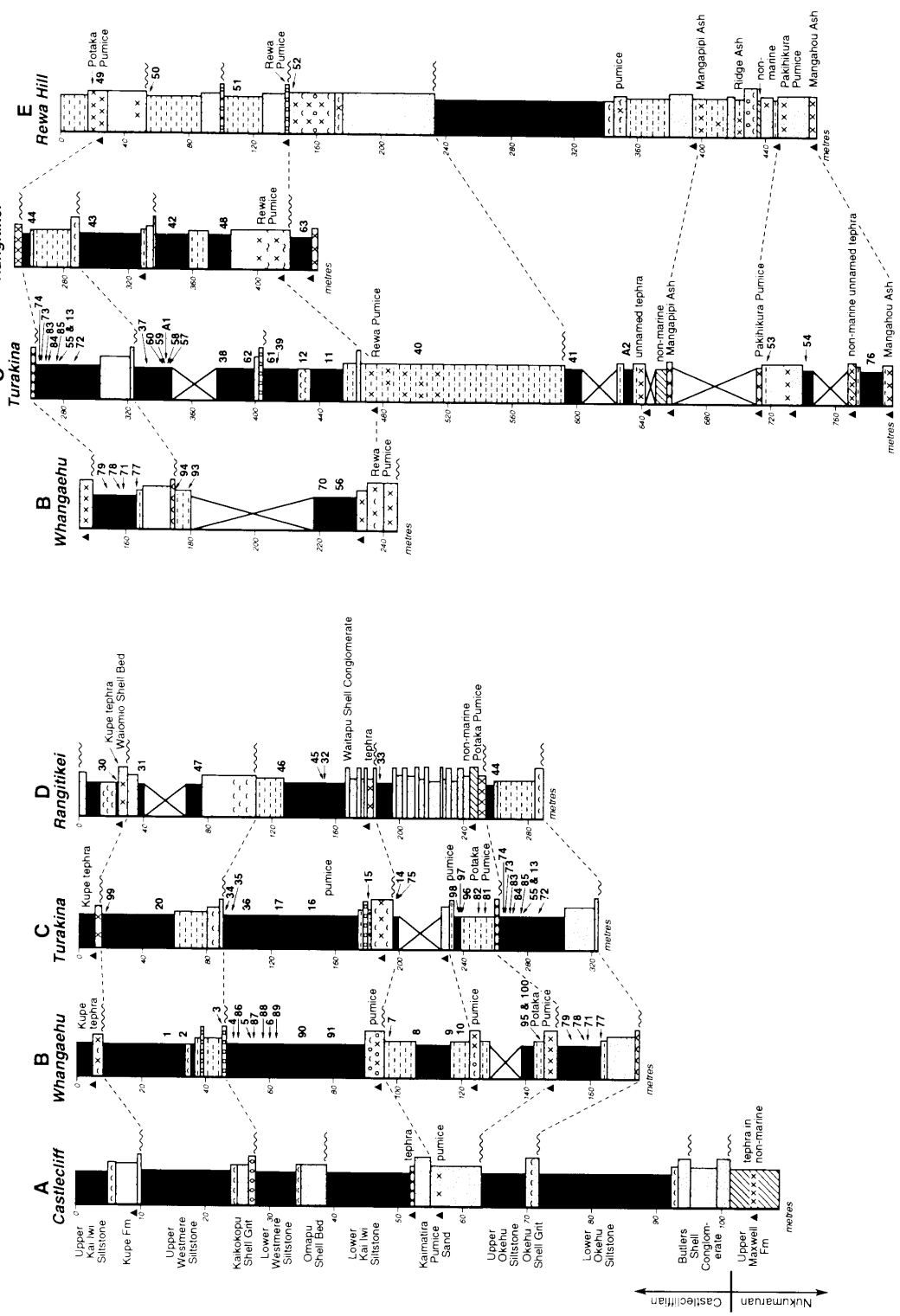

Fig. 3. Lithostratigraphy and stratigraphic subdivision for the (A) Castlecliffian stratotype, (B) Whangaehu River, (C) Turakina River, (D) Rangitikei River and (E) Rewa Hill sections. Stipple = sandstones; solid fill = mudstones and siltstones; dash–dot ornament = interbedded sandstones and siltstones; crosses = tephric horizons. Dashed lines indicate tephrostratigraphic correlations, based on lithostratigraphy and glass chemistry. Palaeomagnetic sampling sites and sampled tephra are indicated by numbers and triangles, respectively. Lithostratigraphy in (E) is after Seward [30]. Stratigraphic thicknesses are in metres.

ance, but chemical fingerprinting of volcanic glass shards [this work], ferromagnesian mineralogy [6] and careful lithostratigraphic correlation allow most to be readily distinguished. The lithostratigraphy, stratigraphic positions and correlation of tuffs across the basin are shown in Fig. 3. In addition to the tuff correlations, the Kupe Formation (containing Kupe tephra), near the top of the studied sequence, contains a distinctive fauna [1,15] which allows confident biostratigraphic correlation across the basin.

Volcanic glass shards in the size range 60–250 μm were separated by wet sieving and magnetic separation using a Frantz Isodynamic Separator. To characterize each tuff, approximately 10–15 representative glass shards were analysed by electron microprobe, using the operating conditions described by Pillans and Wright [16]. Representative analyses of each correlated tuff are given in Table 1. Most of the tuffs are chemically distinguishable from each other on the ternary FeO-CaO-K_2O plot (Fig. 4). Mixed populations of glass shards from two or more eruptions are present at several sites (e.g., Waitapu Shell Conglomerate in section D; Fig. 3). In such cases, the lowest stratigraphic level of a particular glass population is taken to represent the first incoming of the tuff to the basin.

From youngest to oldest, the stratigraphically most important tuffs are: Kupe tephra, Kaukatea Ash, Potaka Pumice, Rewa Pumice, Mangapipi Ash, Pakihikura Pumice and Mangahou Ash. The names of the tuff horizons follow Seward [5,6],

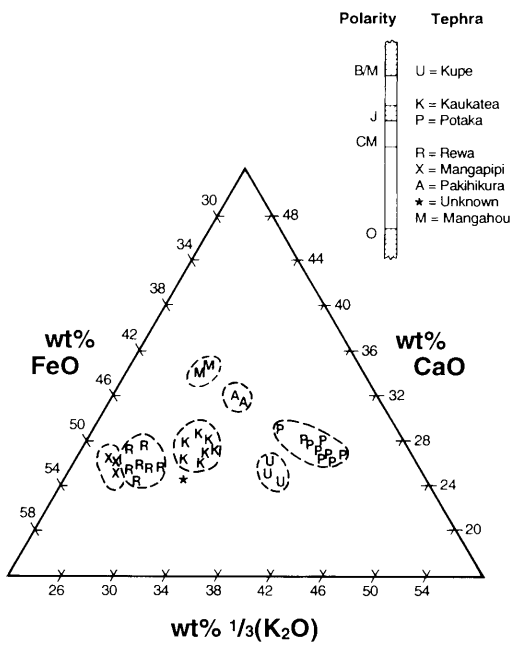

Fig. 4. CaO-FeO-1/3K_2O plot from electron microprobe analyses of volcanic glass shards, Wanganui Basin. Locations and correlation of sampled horizons are shown in Fig. 3.

Table 1
Representative analyses of volcanic glass shards determined by electron microprobe

Name Section	Kupe C	Kaukatea C	Potaka D	Rewa E	Mangapipi C	Pakihikura E	Mangahou E
SiO_2	77.58(.37)	76.27(.39)	77.80(.28)	75.63(.59)	74.95(.27)	78.14(.26)	75.61(.42)
Al_2O_3	12.10(.17)	12.77(.16)	12.12(.15)	12.99(.34)	13.17(.17)	12.33(.15)	13.11(.14)
TiO_2	0.14(.03)	0.22(.03)	0.10(.04)	0.18(.05)	0.18(.03)	0.10(.05)	0.21(.03)
FeO	1.29(.12)	1.63(.15)	1.08(.14)	1.99(.23)	2.29(.12)	1.30(.09)	1.72(.15)
MgO	0.10(.04)	0.16(.03)	0.09(.03)	0.16(.04)	0.13(.02)	0.10(.04)	0.22(.04)
CaO	0.91(.09)	1.07(.06)	0.88(.09)	1.28(.15)	1.17(.06)	1.14(.08)	1.52(.11)
Na_2O	3.80(.16)	4.27(.06)	3.59(.18)	4.25(.19)	4.38(.14)	3.40(.16)	3.66(.14)
K_2O	3.84(.13)	3.40(.25)	4.12(.24)	3.37(.21)	3.56(.18)	3.32(.15)	3.75(.15)
Cl	0.24(.05)	0.21(.03)	0.22(.03)	0.17(.03)	0.18(.02)	0.16(.02)	0.20(.02)
H_2O	3.88(.71)	6.25(1.21)	3.56(1.18)	5.40(1.31)	6.21(1.36)	5.96(1.56)	7.06(.72)
n	11	11	13	13	13	14	13

Analyses made using a JEOL JXA-733 electron microprobe housed at Victoria University of Wellington. A beam current of 80 nA and a 20 μm beam diameter were used for all analyses. All elements calculated on a water-free basis, with H_2O by difference from 100%. All Fe expressed as FeO. Mean and $\pm 1\sigma$ (in parentheses) based on n analyses.

with the exception of Kupe, which is an informal name proposed here.

Glass shards from two tuffs, Potaka Pumice and Pakihikura Pumice, from section D, were dated by the isothermal plateau fission-track (ITPFT) technique [17]. These shards have a narrow compositional range in major element chemistry, indicating that the ITPFT age estimates are based on single glass populations with a strong likelihood of uniform uranium content. ITPFT ages for the Potaka Pumice and Pakihikura Pumice are 1.05 ± 0.05 and 1.63 ± 0.15 Ma, respectively. Both tuffs yield ages significantly older than previously published fission-track age determinations (Table 2; [5,6,18–19]). Full results are presented in Alloway et al. [7]. Partial fading of fission tracks in glass tends to result in calculated glass ages that are anomalously younger than the true age of a sample, but the ITPFT technique corrects for track fading by laboratory heat treatment at 150°C for 30 days [7,17]. We therefore

Table 2
Fission-track dates for tuff horizons in Wanganui Basin

Tuff	Published ages (Ma)	This work (Ma)
Kupe	0.45±0.09(g)	
Waitapu	0.52±0.08(g)	
Kaukatea	0.57±0.08(g)	
Potaka	0.61±0.06(g); 0.64±0.18(z)	1.05±0.05
Rewa	0.74±0.09(g)	
Mangapipi	0.88±0.13(g)	
Pakihikura	1.06±0.16(g); 1.06±0.18(z)	1.63±0.15
Mangahou	1.26±0.17(g)	

Published ages from [5,6,17,18]. (g) = glass; (z) = zircon.

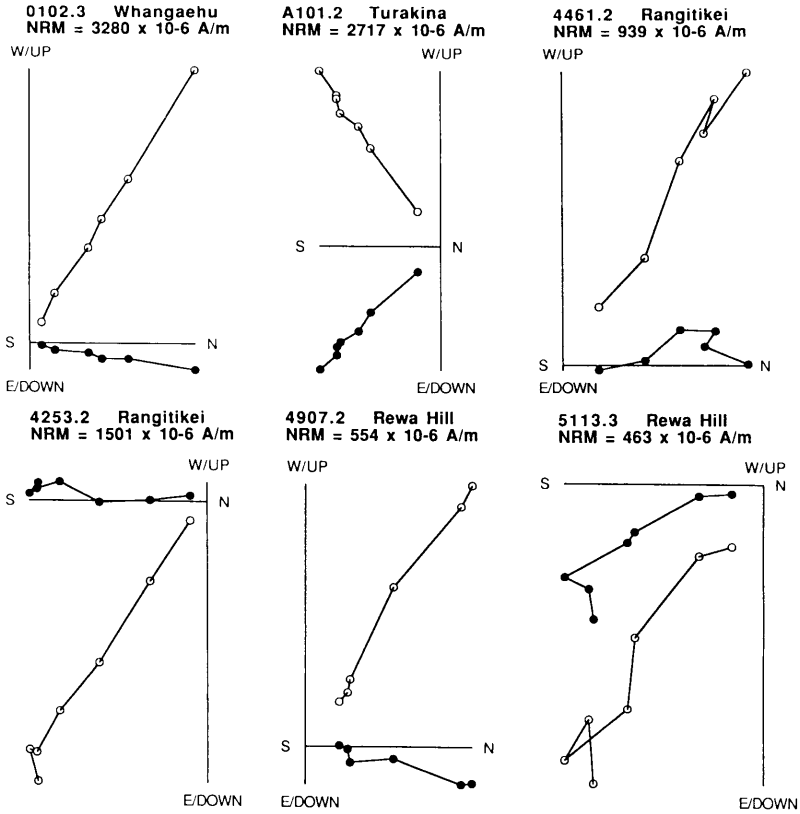

Fig. 5. Vector component plots showing palaeomagnetic behaviour on thermal demagnetization for fine-grained samples from each section studied. ○ = projections onto the vertical plane; ● = projections onto the horizontal plane. Measurements were made at 20, 50, 100, 150, 200, 250, 300 and, in some cases, 350°C. The first two letters of the sample number correspond to the site number, which can be located in Fig. 3 and Appendix 1.

regard the ITPFT ages as more reliable than the previously published glass ages (Table 2).

4. Palaeomagnetic analysis

Conventional palaeomagnetic cores (25 mm in diameter) were drilled at four sections in this study: Whangaehu River, Turakina River, Rangitikei River and Rewa Hill (sections B, C, D and E in Fig. 1, respectively). Given the wide range of sediment grain sizes encountered (e.g., Fig. 2), every effort was made, where possible, to sample the finest grained parts of the sequences, as these sediments are more suitable for palaeomagnetic analysis than coarse-grained sediments. The palaeomagnetic sampling sites are shown in Fig. 3.

Palaeomagnetic samples from the Wanganui Basin are relatively weakly magnetized, with intensities of natural remanent magnetization (NRM) ranging between 0.06 and 3.91 mA/m. Intensities are generally high enough, however, to enable measurement on a Molspin spinner magnetometer (sites 1–54 and 81–100). Sites 55–79 were measured on a two-axis ScT cryogenic magnetometer. Preliminary analyses using stepwise alternating field (AF) and thermal demagnetization techniques indicated that thermal demagnetization is more efficient in removing secondary magnetization components and in isolating primary remanence directions. Many samples displayed spurious behaviour at peak alternating fields above 30 mT while, below this level, sufficient isolation of the characteristic remanence was not achieved. This behaviour has been reported from many such studies of Neogene and Quaternary marine sedimentary sequences in New Zealand [9,20–24]. Thermal demagnetization was therefore used to demagnetize the majority of samples for this study. Several samples from each site were stepwise demagnetized at temperatures of 100, 150, 200, 250, 300 and 350°C. Magnetic susceptibility was measured using a Bartington Instruments M.S.1 susceptibility meter after each demagnetization step to monitor for thermally induced alteration of magnetic minerals. Thermally induced changes in magnetic mineralogy typically occur at temperatures of 350°C and higher and are characterized by a large increase in susceptibility and loss of coherency of the palaeomagnetic signal, possibly because of formation of hyper-fine magnetic phases with short relaxation times and viscous magnetic behaviour. No further demagnetization was carried out when such changes became evident.

Fine-grained samples were generally more stably and intensely magnetized than relatively coarse-grained samples. Vector component plots for fine-grained samples are shown, from each section studied, in Fig. 5. Some samples display extremely stable magnetic behaviour, with virtually no secondary components of magnetization. Most samples show some evidence of a Brunhes Chron viscous overprint which is easily removed, as well as some directional scatter due to the insensitivity of a spinner magnetometer in measuring weakly magnetized samples.

The magnetization of the samples unblocks at relatively low temperatures (i.e., less than 20% of the NRM intensity remains at temperatures of 300–350°C; Fig. 5). Rock-magnetic analyses have been carried out on samples from each section studied and more detailed results are presented elsewhere [24]. The samples were analysed using a technique outlined by Lowrie and Heller [25] and Lowrie [26] in which an isothermal remanent magnetization (IRM) is induced at three different fields (1.4 T, 0.4 T and 0.125 T) along the three orthogonal axes of a sample. The sample is then subjected to stepwise thermal demagnetization at 50°C increments up to 650°C. Application of an IRM at three different fields allows analysis of the thermomagnetic behaviour of a sample over three different ranges of coercivities. Results indicate that the palaeomagnetic signal recorded in the Wanganui Basin is dominated by titanomagnetite (or titanomaghaemite) grains with maximum unblocking temperatures of around 350°–400°C and dominant coercivities in the < 0.125 T range [24]. However, isolated occurrences of ferrimagnetic iron sulphide minerals, that have slightly lower maximum unblocking temperatures, cannot be ruled out. The secondary mineral that forms from thermal alteration above 350°C is usually magnetite with a maximum unblocking temperature of ca. 580°C.

Coarse-grained samples are often strongly overprinted by secondary components of magnetization and thermal demagnetization usually does not isolate primary remanence directions before intensities drop below the noise level of the magnetometer, or before thermal alteration masks the NRM signal. The primary palaeomagnetic polarity is usually clear even though the primary direction has not been isolated. For sites where this type of palaeomagnetic behaviour is observed, the trends described by measurements above the noise limit of the magnetometer constrain great circles of remagnetization which are used to extrapolate to a point where the great circles converge, representing the end point or primary remanence direction for the site [27]. An example is given in Fig. 6 where two samples display normal polarity inclinations that move away from stable normal polarity directions (5008.1 and 5010.1). A third sample displays reversed polarity inclinations that move toward southerly declinations (5009.1). Remagnetization great circles can be fitted accurately to the demagnetization data (Fig. 6A), permitting extrapolation to a well-defined reversed polarity end point (Fig. 6B). This method has been used to obtain site mean remanence directions for all sites that display relatively coherent demagnetization behaviour, but which fail to reach a stable end point. Some coarse-grained sites are too weakly magnetized to enable acquisition of useful palaeomagnetic data and no magnetostratigraphic interpretation can be made from such sites.

Three types of palaeomagnetic behaviour are recognized on the basis of the above discussion and are designated as types A, B and C. Samples that display type-A behaviour are sufficiently stably magnetized to permit the isolation of a characteristic remanence direction from vector component diagrams (e.g., Fig. 5). Samples that display type-B behaviour are less stably magnetized and are overprinted to the extent that remagnetization circle analysis must be used to obtain a site

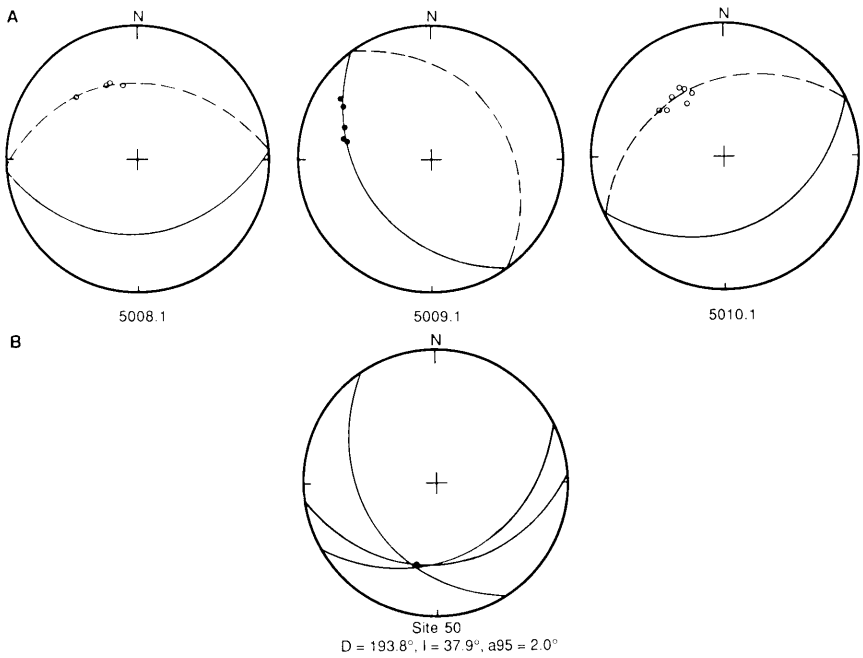

Fig. 6. Example of remagnetization circles analysis for samples from site 50. Great-circle fits to thermal demagnetization data are shown in (A), where the dashed lines and circles (○) indicate upward directed inclinations and solid lines and dots (●) indicate downward directed inclinations. Convergence of the great circles is shown in (B) with the site mean direction and α_{95} calculated using the method of McFadden and McElhinny [27].

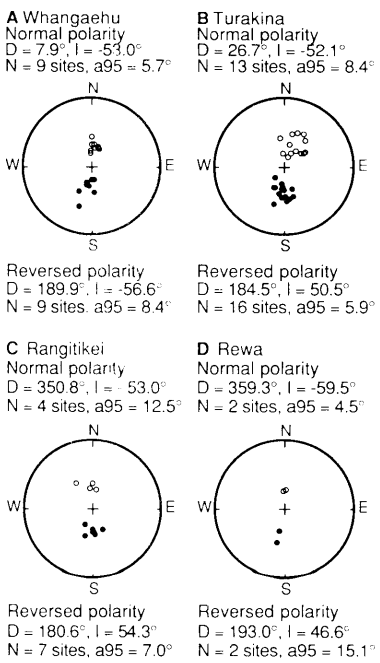

Fig. 7. Equal-angle stereographic projections showing distribution of, and statistics for, palaeomagnetic site mean directions from (A) Whangaehu, (B) Turakina, (C) Rangitikei and (D) Rewa Hill. ○ = normal polarity; ● = reversed polarity.

mean remanence direction (e.g., Fig. 6). Type-C samples are so weakly and unstably magnetized that no useful palaeomagnetic data can be obtained.

Site-averaged remanence directions are plotted on stereographic projections for the four sections studied in Fig. 7. Normal and reversed polarity data are essentially antipodal for each section studied, except for Turakina where normal polarity directions deviate significantly from the axial dipole direction. The majority of the normal polarity directions at Turakina are from the Jaramillo Subchron (see below). This bias away from expected directions could result if persistent non-dipole fields existed during Jaramillo times. Directions from the other sections are generally averaged over much longer periods (except Rewa Hill), and antipodal reversed and normal polarity directions are observed. The reversal test for palaeomagnetic data [28] is therefore satisfied for the majority of the data. Primary remanence directions were isolated from sufficient sites to enable determination of reliable magnetostratigraphic records from all sections studied (Fig. 8). A summary of the palaeomagnetism of each site is given in Appendix 1.

5. Magnetostratigraphy

Magnetostratigraphic columns for each section, including the Castlecliffian stratotype [9], are shown in Fig. 8. The absence of sediment correlative with the glacial stages of the oxygen isotope record is caused by erosion at the sequence-bounding unconformities, but is unlikely to have resulted in time breaks exceeding 30–40 k.y. Therefore, none of the major geomagnetic polarity intervals should be absent. The R-N-R-N polarity zonation obtained at the Turakina and Rangitikei sections is interpreted to represent the upper part of the reversed Matuyama Chron, including the normal Jaramillo Subchron, succeeded by the normal polarity Brunhes Chron. This interpretation is broadly consistent with the zonation and interpretation of Turner and Kamp [9] at the type Castlecliff section (Fig. 8), and is consistent with the ITPFT ages on the Potaka and Pakihikura tephras (Table 2).

At each section, the interpreted position of the Matuyama/Brunhes transition is at the level of the Kaikokopu Shell Grit. From our results in section B, we infer that the transition occurred within the interval of the unconformity at the base of the Kaikokopu Shell Grit, i.e. during a glacial stage. A position within a glacial stage is consistent with the interpreted position of the transition elsewhere in New Zealand [29]. Turner and Kamp [9] interpreted a zone of intermediate field directions above the Kaikokopu Shell Grit at section A as recording the end of the Matuyama/Brunhes transition. However, we do not record transitional directions above the Kaikokopu Shell Grit at other sections (B, C and D; Fig. 8; Appendix 1).

Normal polarity sites occur beneath the first incoming of Potaka Pumice at sections B, C and D. Normal polarity directions are also recorded at sites within Potaka Pumice at sections B, C

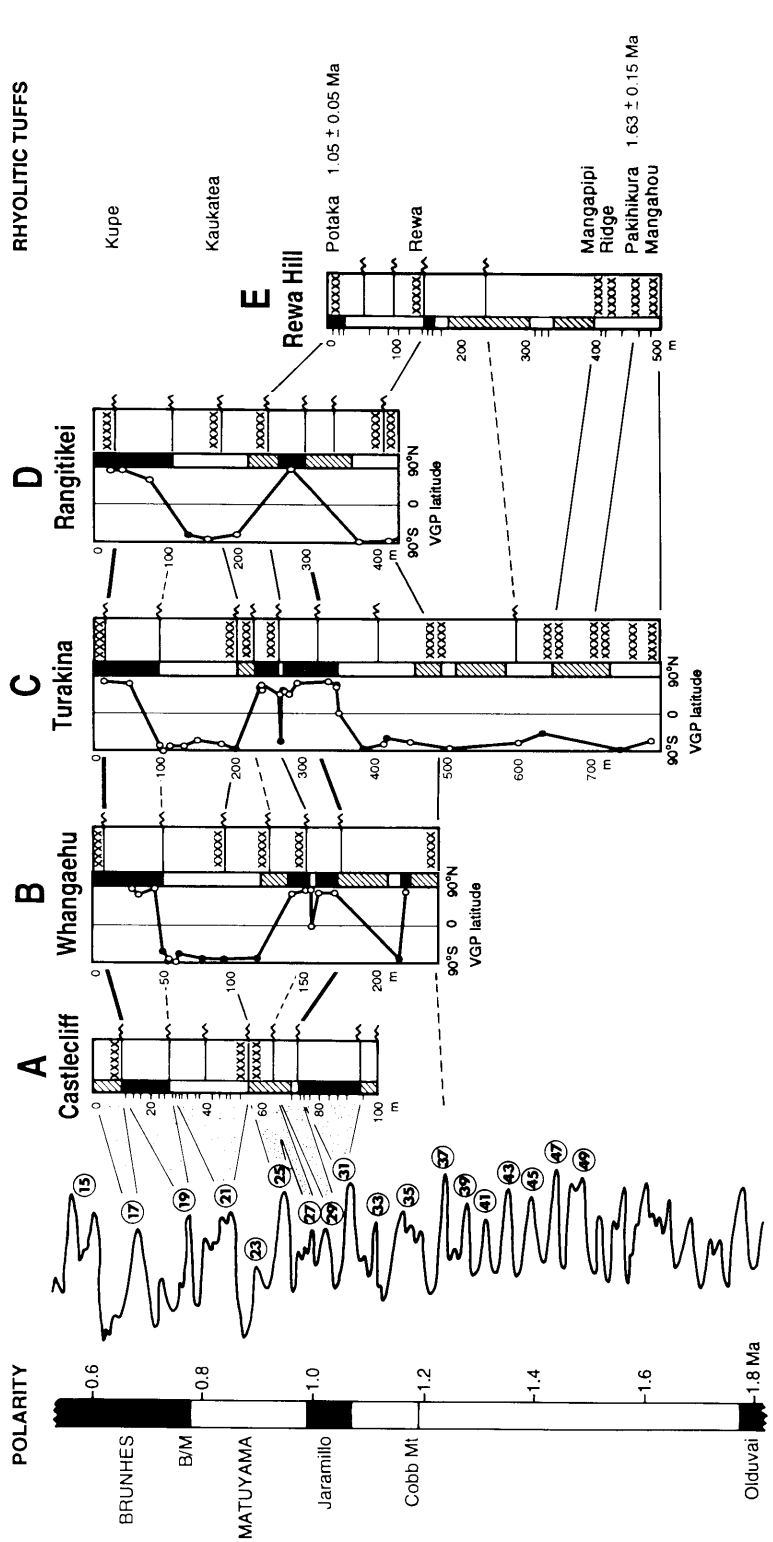

Fig. 8. Correlation of sections in Wanganui Basin with the oxygen isotope record of ODP 677. Thick lines = correlations based mainly on biostratigraphy; thin lines = correlations based mainly on tephrostratigraphy; dashed lines = correlations based mainly on lithostratigraphy. Correlations with the isotope record are based on magnetostratigraphy and interpretation of relative sea-level changes (cf. Fig. 2). Sediments at Wanganui are inferred to represent only odd-numbered stages, with even-numbered stages having been lost in sequence-bounding unconformities. Virtual geomagnetic pole (VGP) latitudes are shown for new sections studied here. Open symbols = data of type A; closed symbols = data of type B; diagonal shading = lack of exposure for sampling or uncertain polarity. Ages of polarity boundaries are from Shackleton et al. [10].

and E. Site A1, some 80 m below Potaka Pumice at section C, yielded a stable intermediate field direction, with reverse polarity sites below and normal polarity sites above (Fig. 8), and is interpreted as the basal Jaramillo transition. This transition was interpreted by Turner and Kamp [9] to coincide with the base of the Butlers Shell Conglomerate at section A. However, the Butlers Shell Conglomerate is part of an incomplete cyclothem, lacking a high-stand systems tract siltstone [14]. We therefore regard it as of little use for correlation of the lower Jaramillo across the Wanganui Basin.

The position of the upper Jaramillo transition is unclear in all sections, but apparently lies between Potaka Pumice and Kaukatea Ash at sections B and C (Fig. 8). Site 73, which lies 3 m below Potaka Pumice at section C, is strongly overprinted, but appears to have a reversed magnetization (Fig. 8 and Appendix 1). Site 71, from 11 m below Potaka Pumice at section B, yielded a transitional field direction (Fig. 8 and Appendix 1). If the normal polarity data from surrounding sites (Appendix 1) represent true geomagnetic directions, sites 71 and 73 may represent a short interval of reversed polarity within the Jaramillo Subchron. Alternatively, sites 49 (section E), 74 and 78 (section C) and 79 (section B) may have been completely overprinted during the Brunhes Chron. At this stage we favour the first interpretation because we believe that sites 49, 74, 78 and 79 all record stable normal polarity directions (e.g., site 49; Fig. 5). We therefore place the upper Jaramillo transition between Potaka Pumice and Kaukatea Ash.

The upper Jaramillo polarity transition at the Castlecliff section was placed by Turner and Kamp [9] at the level of the Okehu Shell Grit (Fig. 3, section A). This position is based on a single site (their site 4) of reversed polarity above the Okehu Shell Grit, in a part of the section that is strongly overprinted. Turner and Kamp [9] were unable to locate suitable palaeomagnetic sites in the immediately overlying strata, including Kaimatira Pumice Sand. Our data from sections B, C, D, and E indicate dominantly normal polarity strata between Okehu Shell Grit and the base of Potaka Pumice (Figs. 3 and 8, and Appendix 1; see above). We have correlated the Okehu Shell Grit across the basin on the basis of its stratigraphic position below Kaimatira Pumice Sand (containing Potaka Pumice), and its faunal assemblage which is dominated at all sections by the shallow water bivalve *Maorimactra*. We therefore conclude that, as for sections B and C, section A may record evidence of a short polarity reversal in the Jaramillo Subchron.

The R-N-R-N polarity sequence at Rewa Hill (section E) was interpreted by Seward [30] to represent the sequence Matuyama–Jaramillo–Matuyama–Brunhes. Our resampling of several sites at Rewa Hill confirms the polarity zonation reported by Seward [30]. The interpretation of Seward [30] is consistent with previously published fission-track ages (Table 2) of several tuffs at Rewa Hill [5,6], but is in conflict with the magnetostratigraphic interpretations of Turner and Kamp [9] and this paper. However, as stated above, low-temperature annealing of glasses can occur, resulting in serious under-estimation of ages [17]. A new fission-track age of 1.05 ± 0.05 Ma reported here on glass shards from the Potaka Pumice at Rewa Hill, using the ITPFT method, is consistent with our polarity interpretation (Fig. 8). Furthermore, the Matuyama/Brunhes transition is located at the level of the Kaikokopu Shell Grit (Fig. 8), some 140 m higher in the sequence than Potaka Pumice in section D. We therefore conclude that the upper zone of normal polarity at Rewa Hill represents the Jaramillo Subchron. Recent revisions of the geomagnetic polarity timescale, based on astronomical calibration of existing timescales [e.g., 31], give a revised age of 0.99 Ma for the top and 1.07 Ma for the base of the Jaramillo Subchron [10,32], consistent within the limits of uncertainty for the above age determination from Potaka Pumice. Note that although the astronomically calibrated isotope record at ODP Site 677 has no direct magnetostratigraphy, the astrochronology for magnetic reversals [10,32] has been confirmed and accepted by Cande and Kent [36]. Astronomical calibration of the ages of geomagnetic reversals is also supported by recent $^{40}Ar/^{39}Ar$ dating of Pleistocene lava flows [33,34] and tephra [35]. Thus the revised dates for polarity boundaries,

given by Shackleton et al. [10] from analysis of ODP Site 677, are accepted in this study.

The lower zone of normal polarity recorded near the Rewa Pumice at section E must therefore lie below the Jaramillo Subchron. It is unlikely to represent the Olduvai Subchron which is recorded lower in the sequence by Seward et al. [37], but is more likely to represent the Cobb Mountain Subchron (1.19 Ma; [10]). This interpretation is confirmed by stable normal polarity data obtained from a site just above the Rewa Pumice at section B (Fig. 8). The long interval of reversed polarity below the Rewa Pumice in sections D and E, which includes the Pakihikura Pumice (1.63 ± 0.15 Ma), is interpreted to represent the middle Matuyama Chron, above the Olduvai Subchron (1.77–1.95 Ma [10]).

6. Correlation of sea-level cycles with the global oxygen isotope timescale

Correlations of the Wanganui sequence with the odd-numbered (interglacial) global isotope stages, and the bounding unconformities with the even-numbered (glacial) stages, have been proposed previously [3,14,38–40]. However, these correlations are based only on the Castlecliff section (A), which is the thinnest and stratigraphically least complete of the sections that we have studied (Fig. 3). Here we use all five studied sections in a proposed correlation with the oxygen isotope stages. In addition, we use the high-resolution, astronomically tuned, isotope record from ODP Site 677 [10] as the reference isotope record to which we make our correlations. Previous correlations (except [14]) were based on older, less-detailed isotope records.

An interpretation of relative sea-level changes for a typical Wanganui cyclothem is summarized in Fig. 2. The sequence boundary represents a period of emergence during glacial low sea level followed by rising relative sea level with erosion in the intertidal zone. Continued rise in relative sea level is represented by sediments of the transgressive systems tract, culminating in a mid-cycle condensed shellbed at, or near, the peak sea-level rise (maximum flooding surface). The upper siltstone (high-stand systems tract, HST) represents seaward progradation of the shore-connected highstand wedge, which downlaps onto the mid-cycle condensed shellbed at the sea-level maximum and the beginning of relative sea-level fall. Usually only the shelf siltstone facies of the HST are preserved; evidence of marked shoaling at the top of the HST is usually absent due to erosion by the next cycle. However, relatively complete shoaling upward HST's have been recognized in the Rangitikei Valley [e.g., 15]. If the relative sea-level changes are broadly accepted as glacio-eustatic in origin [e.g., 3,14], each cyclothem can be inferred to represent the early and middle parts of the odd-numbered isotope stages. Several lines of evidence, summarized by Carter et al. [2], suggest that the cyclothems could not have been produced by tectonic pulses, despite the proximity of the Wanganui Basin to an active plate boundary. Such evidence includes the gentle regional dips and unfaulted nature of the cyclothems over tens of kilometres, and the low rates of tectonic uplift calculated from the ages and elevations of marine terraces within the basin [13].

Our starting point for correlation is the interpreted position of the Matuyama/Brunhes (M/B) transition within the unconformity at the base of the Kaikokopu Shell Grit (Fig. 8). The M/B transition is generally placed close to the stage 19/20 boundary in deep-sea cores [e.g., 10,12], although some authors [41,42] have argued for a position close to the stage 18/19 boundary. The 18/19 position [41,42] is based on the apparent relationship between post-depositional remanent magnetization lock-in depth and sedimentation rates in deep-sea cores. We have investigated possible correlations of the Wanganui sequence using both positions of the M/B transition, but for the reasons outlined below favour the 19/20 position. The 19/20 position is also supported by detailed palaeomagnetic investigations of Chinese loess, where the M/B transition occurs within the upper part of loess L8 [43,44], and magnetic susceptibility variations indicate correlation of loess L8 with isotope stage 20 in deep-sea cores [43]. Although there are uncertainties about the precise timing of magnetization lock-in for both

deep-sea sediments and the Chinese loess, sediment accumulation rates are an order of magnitude higher in the Wanganui Basin than in both of these records, and the position of the M/B transition is unlikely to be similarly affected at Wanganui.

Correlation of the unconformity at the base of the Kaikokopu Shell Grit with isotope stage 20 implies that the sediments in the cyclothem above represent stage 19 and that the cyclothem below represents stage 21. The cycle containing the Kupe Formation would therefore correlate with stage 17. Identification of Kaukatea Ash in the upper part of Kaimatira Pumice Sand at sections A to C, and in Waitapu Shell Conglomerate in section D, clearly establishes that Omapu Shellbed in section A has no lateral lithological correlative in the other sections. It is possible that Omapu Shellbed and the overlying Lower Westmere Siltstone have been completely eroded from the sequence, but comparative sediment thicknesses do not support this interpretation (Fig. 3). We therefore correlate the whole interval from Kaukatea Ash to base Kaikokopu with stage 21, noting that this isotope stage is unusually long compared to adjacent odd-numbered isotope stages in ODP 677.

The next important tie-point for correlation is the basal Jaramillo transition, located within isotope stage 31 in deep-sea cores [10], and located some 80 m below the base of the Potaka Pumice in section C at Wanganui. The position of the transition within high-stand strata at Wanganui is consistent with its placement in mid-stage 31 of the oxygen isotope stratigraphy. Of the four odd-numbered isotope stages between 31 and 21, the stage 23 peak is conspicuously lower than the others, similar in amplitude to stage 3 in the late Brunhes Chron. We suggest therefore that stage 23 may have no record at Wanganui [cf. 14], and infer correlations of the three cyclothems above the basal Jaramillo with stages 25, 27 and 29. On this basis, the upper Jaramillo transition (in stage 27) would lie within the cyclothem containing base Potaka at sections B and C. Potaka Pumice has normal polarity (site 49) at section E, and sites above base Potaka have normal polarity (sites 96, 97, 98 and 100) at sections B and C. A tephra with major-element glass chemistry identical to Potaka Pumice occurs at the 21.50 m depth at DSDP Site 593 in the Tasman Sea ([45]; Fig. 1). A high-resolution oxygen isotope stratigraphy of the core [46] shows that the tephra occurs in isotope stage 28, within the Jaramillo Subchron [47], in excellent agreement with our results from the Wanganui Basin.

Cyclothems below the basal Jaramillo transition are less well defined than those above, and also change in character. Non-marine sediments are more in evidence, and marine sediments are dominated by shallow-water (above wave base) facies, particularly below the Rewa Pumice. Apart from the tuff horizons, and the tentative identification of the Cobb Mountain Subchron in sections B and E, we have not yet established firm correlations of cyclothems between sections. On the basis of the position of the Cobb Mountain Subchron in deep-sea isotope records and in the Wanganui records, we correlate the cyclothem containing the Cobb Mountain Subchron with isotope stage 37. The ITPFT age of 1.63 ± 0.15 Ma for Pakihikura Pumice near the base of section E places a broad constraint on possible correlation with the isotope stratigraphy, but the 1σ age uncertainty spans several isotope stages. We therefore refrain from making detailed correlations with isotope stages for the older parts of the studied sections (Fig. 8).

7. Conclusions

Magnetostratigraphic results provide confirmation of the tephrostratigraphic correlation given in Fig. 3. Previously published fission-track ages for Wanganui Basin tuffs [5,6,18,19] represent gross under-estimations of the true ages, due to low-temperature annealing of glass shards in these horizons. The Matuyama/Brunhes geomagnetic polarity transition is closely associated with the Kaikokopu Shell Grit at all localities studied. The base of the Jaramillo Subchron lies beneath the Potaka Pumice at all sections, and at one section (C) the basal transition of the Jaramillo Subchron is recorded in high-stand systems tract siltstone. The top of the Jaramillo Subchron appears to lie

above the first incoming of Potaka Pumice (dated at 1.05 ± 0.05 Ma; [7]) and below Kaukatea Ash (undated). The Potaka Pumice therefore provides important constraints on the age of the upper Jaramillo polarity transition. A possible short interval of reversed polarity occurs in three sections within the Jaramillo. Rewa Pumice (undated) lies close to a zone of normal polarity proposed as a correlative to the Cobb Mountain Subchron. Future dating of the Rewa Pumice may provide useful constraints on the age of the Cobb Mountain Subchron. The Pakihikura Pumice, dated at 1.63 ± 0.15 Ma, in the lower part of the studied sequences, lies above the Olduvai Subchron.

On the basis of magnetostratigraphy and isothermal plateau fission-track ages, we make correlations of cyclothems at Wanganui with oxygen isotope stages 17–31. The Castlecliffian stratotype section is shown to be incomplete compared to other sections in the Wanganui Basin. Below stage 31 (base Jaramillo), the character of cyclothems changes at Wanganui. Beu and Edwards [3] also noted this change in character, which is mirrored by a change in amplitude and frequency of oxygen isotope records at about the same time [48]. However, the dominance of nonmarine and nearshore marine sediments in Wanganui Basin below the Jaramillo, as compared with dominantly nearshore and offshore marine sediments above, cannot be entirely explained by glacioeustatic changes. We suggest that regional tectonic changes, associated with the initiation of uplift of the main axial mountain ranges to the east of the basin at about 1 Ma [29,49], played a major role in changing the cyclothemic character. We are investigating further the nature of cyclothems in the basin below the Jaramillo Subchron, in order to better understand their relationships to climate and sea-level changes inferred in deep-sea cores.

Acknowledgements

We are grateful to Janice Fong and Sally Rowe for draughting several of the figures and to Allister Gorman for carrying out some of the palaeomagnetic analyses. ITPFT dates were determined at the Geology Department, University of Toronto, and funded by the Natural Sciences and Engineering Research Council of Canada. Fieldwork by BJP and GSW and the costs of palaeomagnetic analysis were supported by the Internal Grants Committee, Victoria University of Wellington. STA was funded by an Australian Postgraduate Research Award and Australian Research Council grants awarded to the Marine Geoscience Group, James Cook University of North Queensland.

Appendix 1
Summary of palaeomagnetic data from each section studied

Turakina section

Site	Thickness (m)	n/N	D (°)	I (°)	NRM (mA/m)	α95 (°)	κ	SP	GC	Type	Polarity
99	17	5/5	357.1	-67.6	2.91	2.2	809	5	-	A	N
20	51	4/4	21.9	-64.6	0.38	4.7	218	4	-	A	N
34	92	4/9	160.2	52.8	0.08	13.2	28	4	-	A	R
35	96	8/10	183.8	57.8	0.11	7.7	-	5	3	A/B	R
36	105	8/9	190.4	46.7	0.11	4.1	144	8	-	A	R
17	125	1/5	178.0	43.0	0.38	-	-	1	-	A	R
16	145	4/4	196.3	32.3	0.13	3.7	365	4	-	A	R
15	181	2/3	170.0	39.6	0.09	17.3	33	2	-	A	R
14	198	0/5	-	-	0.14	-	-	-	-	C	R?
75	199	5/5	187.0	55.6	0.09	3.2	-	-	5	B	R
98	237	5/5	21.5	-34.3	0.81	5.4	137	5	-	A	N
97	238	3/3	30.0	-32.7	1.74	10.6	58	3	-	A	N
96	239	4/4	13.1	-37.8	1.54	6.1	131	4	-	A	N
74	264	3/3	52.9	-49.8	0.67	22.4	13	3	-	A	N
73	266	4/5	207.2	53.0	0.37	3.5	-	-	4	B	R
83	269	6/6	37.4	-38.7	0.64	13.7	17	6	-	A	N
84	271	5/5	49.1	-54.1	0.32	19.8	10	5	-	A	N
85	276	4/6	55.6	-52.0	0.42	7.9	79	4	-	A	N
55	277	0/2	-	-	0.27	-	-	-	-	C	?
13	277	0/5	-	-	0.21	-	-	-	-	C	?
72	287	5/5	351.3	-44.0	0.94	29.6	5	5	-	A	N
37	332	9/9	13.9	-52.3	0.26	5.1	83	9	-	A	N
60	342	5/5	19.0	-71.6	0.21	18.0	12	5	-	A	N
59	343	5/5	35.0	-57.5	0.27	7.2	75	5	-	A	N
A1	344	9/12	118.6	-49.2	0.55	9.9	22	9	-	A	T
58	345	0/5	-	-	0.16	-	-	-	-	C	?
57	346	0/5	-	-	0.15	-	-	-	-	C	?
38	379	4/8	187.9	62.1	0.12	2.3	-	-	4	B	R
62	394	0/4	-	-	0.25	-	-	-	-	C	?
61	409	4/4	185.9	41.8	0.14	9.2	-	3	1	A/B	R
39	413	3/8	222.0	68.6	0.06	8.4	-	-	3	B	R
12	430	0/5	-	-	0.26	-	-	-	-	C	?
11	447	3/3	164.0	42.5	0.24	12.0	45	3	-	A	R
40	502	10/10	181.0	52.3	0.10	7.7	-	5	5	A/B	R
41	598	3/5	204.2	53.8	0.06	15.7	27	3	-	A	R
A2	631	4/8	129.9	45.5	0.17	1.6	-	-	4	B	R
53	717	0/6	-	-	0.21	-	-	-	-	C	R?
54	742	4/8	182.3	56.4	0.18	1.9	-	-	4	B	R
76	782	5/5	175.5	36.0	0.30	9.0	48	5	-	A	R

Rewa Hill section

Site	Thickness (m)	n/N	D (°)	I (°)	NRM (mA/m)	α95 (°)	κ	SP	GC	Type	Polarity
49	25	9/9	3.8	-58.3	0.58	3.5	174	9	-	A	N
50	55	3/3	193.8	37.9	0.52	2.0	-	-	3	B	R
51	110	13/13	192.0	55.3	0.28	7.0	31	13	-	A	R
52	145	10/10	354.5	-60.5	1.18	3.0	213	10	-	A	N

Appendix 1 (continued)

Whangaehu section

Site	Thickness (m)	n/N	D (°)	I (°)	NRM (mA/m)	α95 (°)	κ	SP	GC	Type	Polarity
1	28	4/4	9.3	-57.7	3.42	3.5	404	4	-	A	N
2	33	3/4	24.0	-57.9	0.37	28.3	8	3	-	A	N
3	45	5/5	356.1	-63.2	0.31	8.5	54	5	-	A	N
4	48	0/5	-	-	0.10	-	-	-	-	C	R?
86	50	5/5	197.4	27.6	0.50	2.1	-	-	5	B	R
5	54	5/6	193.7	61.1	0.25	5.3	-	-	5	B	R
87	55	5/5	173.4	49.0	0.20	9.8	-	3	2	A/B	R
88	58	0/5	-	-	0.26	-	-	-	-	C	R?
6	60	3/3	186.1	59.2	0.37	13.7	35	3	-	A	R
89	62	5/5	206.3	46.6	0.41	1.8	-	-	5	B	R
90	70	0/5	-	-	1.47	-	-	-	-	C	?
91	79	5/5	167.1	67.7	0.24	4.5	-	-	5	B	R
7	96	5/5	178.7	68.0	0.37	6.1	-	-	5	B	R
8	106	0/4	-	-	0.32	-	-	-	-	C	R?
9	116	0/5	-	-	0.11	-	-	-	-	C	R?
10	119	2/2	197.8	63.6	0.24	-	-	-	2	B	R
100	144	5/5	0.4	-37.6	1.08	9.6	42	5	-	A	N
79	154	5/5	6.7	-52.2	0.25	7.5	70	5	-	A	N
78	158	5/5	1.1	-52.4	0.34	8.1	60	5	-	A	N
71	159	4/5	115.8	-39.2	0.40	9.1	59	4	-	A	T
77	163	5/5	18.2	-54.6	0.52	9.7	42	5	-	A	N
94	175	5/5	0.8	-41.8	0.45	5.1	151	5	-	A	N
70	221	5/5	194.5	60.0	0.21	3.7	-	-	5	B	R
56	226	6/6	19.5	-56.5	0.39	3.7	245	6	-	A	N

Rangitikei section

Site	Thickness (m)	n/N	D (°)	I (°)	NRM (mA/m)	α95 (°)	κ	SP	GC	Type	Polarity
30	26	10/14	12.8	-58.3	0.46	10.0	20	10	-	A	N
31	39	9/13	0.2	-50.0	0.22	5.9	62	9	-	A	N
47	74	2/9	326.5	-41.5	0.11	54.3	3	2	-	A	N
46	126	5/5	196.4	46.0	0.09	6.4	-	-	5	B	R
45	152	6/6	174.5	50.0	0.49	5.2	123	6	-	A	R
32	153	4/7	181.2	53.1	0.15	5.9	-	1	3	A/B	R
33	188	4/10	205.0	61.4	0.18	13.2	-	1	3	A/B	R
44	260	9/9	351.5	-57.0	0.88	3.9	144	9	-	A	N
43	297	0/4	-	-	0.08	-	-	-	-	C	?
42	347	9/10	179.2	57.8	1.58	2.7	304	9	-	A	R
48	379	3/9	177.1	52.7	0.31	6.1	173	3	-	A	R
63	429	5/5	153.7	52.9	0.24	12.1	-	3	2	A/B	R

References

[1] C.A. Fleming, The geology of the Wanganui subdivision, N.Z. Geol. Surv. Bull. 52, 1953.

[2] R.M. Carter, S.T. Abbott, C.S. Fulthorpe, D.W. Haywick and R.A. Henderson, Application of global sea level and sequence stratigraphic models in Southern Hemisphere Neogene strata from New Zealand, in: Sedimentation, Tectonics and Eustasy: Sea Level Changes at Active Margins, D.I.M. MacDonald, ed., Int. Assoc. Sedimentol. Spec. Publ. 12, 41–65, 1991.

[3] A.G. Beu and A.R. Edwards, New Zealand Pleistocene and late Pliocene glacio-eustatic cycles, Palaeogeogr. Palaeoclimatol. Palaeoecol. 46, 119–142, 1984.

[4] B. Pillans, S.T. Abbott, A.G. Beu and R.M. Carter, A possible Lower/Middle Pleistocene boundary stratotype in Wanganui Basin, New Zealand, Abstr. Int. Union Quat. Res. (Beijing), p. 281, 1991.

[5] D. Seward, Age of New Zealand Pleistocene substages by fission-track dating of glass shards from tephra horizons, Earth Planet. Sci. Lett. 24, 242–248, 1974.

[6] D. Seward, Tephrostratigraphy of the marine sediments in the Wanganui Basin, New Zealand, N.Z.J. Geol. Geophys. 19, 9–20, 1976.

[7] B.V. Alloway, B.J. Pillans, A.S. Sandhu and J.A. Westgate, Revision of the marine chronology in Wanganui Basin, New Zealand, based on the isothermal plateau fission-track dating of tephra horizons, Sediment. Geol., 82, 299–310, 1993.

[8] K.F. Stevens and P.P. Vella, Palaeoclimatic interpretation of stable isotope ratios in molluscan fossils from middle Pleistocene marine strata, Wanganui, New Zealand, Palaeogeogr. Palaeoclimatol. Palaeoecol. 34, 257–265, 1981.

[9] G.M. Turner and P.J.J. Kamp, Palaeomagnetic location of the Jaramillo subchron and the Matuyama–Brunhes transition in the Castlecliffian stratotype section, Wanganui Basin, New Zealand, Earth Planet. Sci. Lett. 100, 42–50, 1990.

[10] N.J. Shackleton, A. Berger and W.R. Peltier, An alternative astronomical calibration of the lower Pleistocene timescale based on ODP Site 677, Trans. R. Soc. Edinb. 81, 251–261, 1990.

[11] T.A. Stern and F.J. Davey, Crustal structure and origin of basins formed behind the Hikurangi subduction zone, New Zealand, in: Origin and Evolution of Sedimentary Basins and their Energy and Mineral Resources, R.A. Price, ed., Am. Geophys. Union Geophys. Monogr. 48, 73–85, 1989.

[12] N.J. Shackleton and N.D. Opdyke, Oxygen isotope and palaeomagnetic stratigraphy of equatorial Pacific core V28–238: oxygen isotope temperatures and ice volumes on a 10^5 and 10^6 year scale, Quat. Res. 3, 39–55, 1973.

[13] B. Pillans, Upper Quaternary marine terrace chronology and deformation, South Taranaki, New Zealand, Geology 11, 292–297, 1983.

[14] S.T. Abbott and R.M. Carter, The sequence architecture of mid-Pleistocene (c 1.1–0.4 Ma) cyclothems from New Zealand: facies development during a period of orbital control on sea level cyclicity, in: Orbital Forcing and Cyclic Sequences, P.L. de Boer and D.G. Smith, eds., Int. Assoc. Sedimentol. Spec. Publ., in press, 1993.

[15] S.T. Abbott, The Mid-Pleistocene Waiomio Shellbed (Castlecliffian, c. 550–600 ky), Wanganui Basin, New Zealand, Alcheringa 16, 171–180, 1992.

[16] B. Pillans and I. Wright, Late Quaternary tephrostratigraphy from the southern Havre Trough–Bay of Plenty, northeast New Zealand, N.Z.J. Geol. Geophys. 35, 129–143, 1992.

[17] J.A. Westgate, Isothermal plateau fission-track ages of hydrated glass shards from silicic tephra beds, Earth Planet. Sci. Lett. 95, 226–234, 1989.

[18] J.D. Boellstorff and M.T. Te Punga, Fission-track ages and correlation of Middle and Lower Pleistocene sequences from Nebraska and New Zealand, N.Z.J. Geol. Geophys. 20, 47–58, 1977.

[19] D. Seward, Comparison of zircon and glass fission-track ages from tephra horizons, Geology 7, 479–482, 1979.

[20] J.P. Kennett and N.D. Watkins, Late Miocene–Early Pliocene paleomagnetic stratigraphy, paleoclimatology and biostratigraphy in New Zealand, Bull. Geol. Soc. Am. 85, 1385–1398, 1974.

[21] I.C. Wright and P.P. Vella, A New Zealand Late Miocene magnetostratigraphy: glacioeustatic and biostratigraphic correlations, Earth Planet. Sci. Lett. 87, 193–204, 1988.

[22] G.M. Turner, A.P. Roberts, C. Laj, C. Kissel, A. Mazaud, S. Guitton and D.A. Christoffel, New paleomagnetic results from Blind River: revised magnetostratigraphy and tectonic rotation of the Marlborough region, South Island, N.Z.J. Geol. Geophys. 32, 191–196, 1989.

[23] A.P. Roberts and G.M. Turner, Diagenetic formation of ferrimagnetic iron sulphide minerals in rapidly deposited marine sediments, South Island, New Zealand, Earth Planet. Sci. Lett. 115, 257–273, 1993.

[24] A.P. Roberts and B.J. Pillans, Rock magnetism of Lower/Middle Pleistocene marine sediments, Wanganui Basin, New Zealand, Geophys. Res. Lett. 20, 839–842, 1993.

[25] W. Lowrie and F. Heller, Magnetic properties of marine limestones, Rev. Geophys. Space Phys. 20, 171–192, 1982.

[26] W. Lowrie, Identification of ferromagnetic minerals in a rock by coercivity and unblocking temperature properties, Geophys. Res. Lett. 17, 159–162, 1990.

[27] P.L. McFadden and M.W. McElhinny, The combined analysis of remagnetization circles and direct observations in palaeomagnetism, Earth Planet. Sci. Lett. 87, 161–172, 1988.

[28] P.L. McFadden and M.W. McElhinny, Classification of the reversal test in palaeomagnetism, Geophys. J. Int. 103, 725–729, 1990.

[29] T. Black, Chronology of the Middle Pleistocene Kidnappers Group, New Zealand and correlation to global oxygen isotope stratigraphy, Earth Planet. Sci. Lett. 109, 573–584, 1992.

[30] D. Seward, Some aspects of sedimentology of the Wanganui Basin, North Island, New Zealand, Ph.D. Thesis, Victoria Univ. Wellington, 1974 (Unpubl.).
[31] W.A. Berggren, D.V. Kent and J.A. Van Couvering, The Neogene: Part 2. Neogene geochronology and chronostratigraphy, in: Geochronology and the Geological Timescale, N.J. Snelling, ed., Geol. Soc. London Mem. 10, 211–260, 1985.
[32] F.J. Hilgen, Astronomical calibration of Gauss to Matuyama sapropels in the Mediterranean and implications for the geomagnetic polarity timescale, Earth Planet. Sci. Lett. 104, 226–224, 1991.
[33] A.K. Baksi, V. Hsu, M.O. McWilliams and E. Farrar, $^{40}Ar/^{39}Ar$ dating of the Brunhes–Matuyama geomagnetic field reversal, Science 256, 356–357, 1992.
[34] T.L. Spell and I. MacDougall, Revisions to the age of the Brunhes–Matuyama boundary and the Pleistocene geomagnetic polarity timescale, Geophys. Res. Lett. 19, 1181–1184, 1992.
[35] L. Tauxe, A.D. Deino, A.K. Behrensmeyer and R. Potts, Pinning down the Brunhes/Matuyama and upper Jaramillo boundaries: a reconciliation of orbital and isotopic time scales, Earth Planet. Sci. Lett. 109, 561–572, 1992.
[36] S.C. Cande and D.V. Kent, A new geomagnetic polarity time scale for the Late Cretaceous and Cenozoic, J. Geophys. Res. 97, 13917–13951, 1992.
[37] D. Seward, D.A. Christoffel and B. Lienert, Magnetic polarity stratigraphy of a Plio-Pleistocene marine sequence of North Island, New Zealand, Earth Planet. Sci. Lett. 80, 353–360, 1986.
[38] A.G. Beu, A.R. Edwards and B. Pillans, A review of New Zealand Pleistocene stratigraphy, with emphasis on the marine rocks, in: Proc. 1st Int. Colloq. Quat. Stratigraphy of Asia and the Pacific Area, M. Osaka,?. Itihara and T. Kamei, eds., pp. 250–269, 1987.
[39] P.J.J. Kamp and G.M. Turner, Pleistocene unconformity-bounded shelf sequences (Wanganui Basin, New Zealand), correlated with global isotope record, Sediment. Geol. 68, 155–161, 1990.
[40] B. Pillans, New Zealand Quaternary stratigraphy: a review, Quat. Sci. Rev. 10, 405–418, 1991.
[41] P.B. deMenocal, W.F Ruddiman and D.V. Kent, Depth of post-depositional remanence acquisition in deep-sea sediments: a case study of the Brunhes–Matuyama reversal and oxygen isotopic stage 19.1, Earth Planet. Sci. Lett. 99, 1–13, 1990.
[42] D.A. Schneider, D.V. Kent and G.A. Mello, A detailed chronology of the Australasian impact event, the Brunhes–Matuyama geomagnetic polarity reversal, and global climate change, Earth Planet. Sci. Lett. 111, 395–405, 1992.
[43] G. Kukla, Loess stratigraphy in Central China, Quat. Sci. Rev. 6, 191–219, 1987.
[44] R. Zhu, Z. Ding, H. Wu, B. Huang and L. Jiang, Details of magnetic polarity transition recorded in Chinese loess, J. Geomag. Geoelectr. 45, 289–299, 1993.
[45] C.S. Nelson, P.C. Froggatt and G.J. Gosson, Nature, chemistry, and origin of late Cenozoic megascopic tephras in Leg 90 cores from the Southwest Pacific, Init. Rep. DSDP 90, 1161–1173, 1985.
[46] C.S. Nelson, C.H. Hendy and A.M. Cuthbertson, Compendium of stable oxygen and carbon isotope data for the late Quaternary interval of deep-sea cores from the Tasman Sea and Southwest Pacific Ocean, Occas. Rep. Dep. Earth Sci., Univ. Waikato, N.Z., No. 16, 1993.
[47] C.E. Barton and J. Bloemendal, Paleomagnetism of sediments collected during Leg 90, Southwest Pacific, Init. Rep. DSDP 90, 1273–1316, 1985.
[48] D.F. Williams, W.S. Moore and R.H. Fillon, Role of glacial Arctic Ocean ice sheets in Pleistocene oxygen isotope and sea level records, Earth Planet. Sci. Lett. 56, 157–166, 1981.
[49] P.A.R. Shane, Remobilised silicic tuffs in middle Pleistocene fluvial sediments, southern North Island, New Zealand, N.Z.J. Geol. Geophys. 34, 489–500, 1991.